NASA TECHNICAL MEMORANDUM

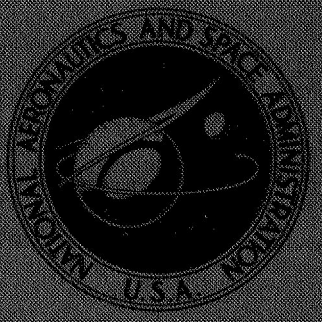

NASA TM X-3304

NASA TM X-3304

PERFORMANCE OF A J85-13 COMPRESSOR WITH CLEAN AND DISTORTED INLET FLOW

Edward J. Milner and Leon M. Wenzel

Lewis Research Center
Cleveland, Ohio 44135

NATIONAL AERONAUTICS AND SPACE ADMINISTRATION • WASHINGTON, D. C. • DECEMBER 1975

1. Report No.	2. Government Accession No.	3. Recipient's Catalog No.
NASA TM X-3304		

4. Title and Subtitle	5. Report Date
PERFORMANCE OF A J85-13 COMPRESSOR WITH CLEAN AND DISTORTED INLET FLOW	December 1975
	6. Performing Organization Code
7. Author(s)	8. Performing Organization Report No.
Edward J. Milner and Leon M. Wenzel	E-8311
	10. Work Unit No.
9. Performing Organization Name and Address	505-05
Lewis Research Center National Aeronautics and Space Administration Cleveland, Ohio 44135	11. Contract or Grant No.
	13. Type of Report and Period Covered
12. Sponsoring Agency Name and Address	Technical Memorandum
National Aeronautics and Space Administration Washington, D.C. 20546	14. Sponsoring Agency Code

15. Supplementary Notes

16. Abstract

The results presented are of a series of experimental tests in which a General Electric J85-13 turbojet engine was subjected to both distorted and undistorted inlet total-pressure conditions. A distinctive feature of the data base obtained is that it includes compressor interstage information not previously recorded for a J85-13 engine. Each of the eight compressor stages was instrumented to obtain the characteristics of the individual stages for undistorted inlet conditions, and these data are documented in the report along with the undistorted compressor overall performance. Also included in the report is the overall performance of the compressor exposed to 14 different distorted-inlet conditions - 10 circumferential patterns and 4 radial patterns. The distortion patterns were introduced using screens that spoiled from 8 to 50 percent of the compressor face area; the distortion screen density, or the area blocked by the screen wire per unit area of screen, varied from 26 to 69 percent.

17. Key Words (Suggested by Author(s))

Compressor stage characteristics
Multistage compressor characteristics
Compressor distortion data

18. Distribution Statement

Unclassified - unlimited
STAR category 07 (rev.)

19. Security Classif. (of this report)	20. Security Classif. (of this page)	21. No. of Pages	22. Price*
Unclassified	Unclassified	32	$3.75

* For sale by the National Technical Information Service, Springfield, Virginia 22161

PERFORMANCE OF A J85-13 COMPRESSOR WITH CLEAN AND DISTORTED INLET FLOW

by Edward J. Milner and Leon M. Wenzel

Lewis Research Center

SUMMARY

A General Electric J85-13 turbojet engine was subjected to both distorted and undistorted inlet total-pressure conditions in a series of experimental tests in an altitude chamber at Lewis Research Center. The data base obtained in those tests and documented in this report is different from any other presently available insofar as it includes individual compressor stage information not previously recorded for a J85-13 engine. Each of the eight compressor stages was instrumented to obtain the characteristics of the individual stages. Presented in this report are the experimental stage characteristic data and curves obtained for an undistorted inlet, as well as the overall compressor performance for undistorted inlet flow. These data are required to assemble a stage-by-stage simulation of the test engine for the purpose of studying dynamic distortion and predicting compressor surge.

In addition, subsequent experimental tests in this series introduced 14 different distortion patterns at the face of the compressor using screens of varying densities and patterns. The study included 10 circumferential and 4 radial distortion patterns, each with a spoiled area which ranged from 8 to 50 percent of the compressor-face total area. The density of the distortion screen varied from 26 to 69 percent. The performance of the distorted compressor at each configuration is presented and compared with the clean-inlet compressor map. These data are presented to form a complete data base which may be used in further investigations of the effects of inlet distortion on the surge margin of the J85 compressor.

INTRODUCTION

Today's trend toward engines with higher thrust and lighter weight has accentuated a problem area in designing modern compressors. An optimum design would be for each stage of the compressor to operate at or near its maximum efficiency with suitable

stall margin as required by the individual stages. However, the adverse effect of inlet distortion on compressor-surge margin has been a persistent problem in obtaining the efficient multistage compressors needed to build the streamlined, high-performance engines demanded today (see, for example, refs. 1 to 4).

Computer simulations of compressors which yield estimates of performance and stability can be very helpful in the compressor design process. References 5 and 6 document techniques used by Willoh and Seldner to simulate an engine with a multistage compressor on an analog computer. It was found that the characteristics of each stage of the compressor had to be included in order to obtain a simulation that could accurately predict the compressor surge line for steady-state flow conditions.

More recently the Routh-Hurwitz method has been used in conjunction with a similar compressor simulation programmed on the digital computer to investigate steady-state compressor stability (ref. 7). Also required in this technique are the characteristics of the individual stages of the compressor being investigated.

Part of a recent experimental program at Lewis was designed to study the effects of casing treatment on compressor performance and stability (ref. 8). Tests were conducted in an altitude chamber using a General Electric J85-13 turbojet engine. Since the casing treatment study required pressure and temperature instrumentation in each of the eight compressor stages, the test rig in its untreated compressor configuration offered an excellent opportunity to create a distortion data base different from any other presently available. The data base would contain not only performance information for the compressor exposed to both distorted and undistorted inlet-pressure patterns, but also interstage data necessary to determine the individual compressor stage characteristics of the test engine.

The purpose of this report is to document experimental data obtained from those tests. The compressor stage characteristics and overall performance obtained in the experimental program for undistorted inlet flow will be presented. In addition, the results of a series of experimental distortion tests will be presented to form a complete data base that may be used in further investigations of the effects of inlet distortion on compressor performance and stability.

Pressure distortions were introduced at the compressor face by means of screens of varying densities and patterns. For each distortion screen pattern the engine nozzle area was decreased until either compressor surge occurred or the turbine temperature limit was reached. As nozzle area was decreased in these tests, fuel flow was manually adjusted to maintain constant corrected rotor speed. At various discrete points in this process steady-state pressures and temperatures for each compressor stage were recorded.

This report is arranged in the following manner. The experimental apparatus and the test procedure are described first. Then the experimental compressor stage char-

acteristic data obtained from clean inlet test conditions are presented along with stage characteristic curves determined from these interstage data. The overall compressor map obtained by using the stage characteristic data is presented and compared with the experimental overall compressor map for undistorted inlet flow. Then the results of the experimental distortion tests are presented. Ten circumferential distortion patterns and four radial distortion patterns were investigated. Surge points for each corrected speed are also presented.

APPARATUS AND PROCEDURE

Tests were conducted in an altitude chamber using a General Electric J85-13 turbojet engine. This engine has an eight-stage axial-flow compressor equipped with three interstage bleeds which open and close in unison. The compressor is directly coupled to a two-stage turbine. The engine also has an afterburner section and an exhaust nozzle with a variable throat area. The combustor is of the through-flow annular type.

Located in the engine inlet are variable guide vanes which are mechanically linked to the interstage bleeds in such a way that the bleeds will be fully opened when the inlet guide vanes are positioned at their maximum angle. For this study the interstage bleeds were scheduled to be fully open below 80 percent corrected speed, half-open at 87 percent corrected speed, and fully closed above 94 percent corrected speed. The turbine diaphragm area was reduced for this particular test engine to 232 square centimeters. The reduced turbine diaphragm area was needed to allow the compressor to surge without exceeding maximum temperature limits.

Part of the experimental program consisted of a series of tests to investigate the effect of casing treatment on compressor performance and stability (ref. 8). However, for the casing treatment study a special compressor case was needed. It was machined to accept removable, grooved inserts to be used in those experimental tests and is described fully in the casing treatment report. For normal operation a set of solid untreated rings could be inserted in the compressor case. The experimental data to be presented in this report were obtained using the normal operation configuration.

Instrumentation

The compressor face was instrumented with 12 rakes of 5 total-pressure taps each. The pressure taps along a rake were not linearly spaced. The spacing had been adjusted so that each pressure tap represented an equal portion of the cross-sectional area of the compressor. Hence, no special significance had to be attached to the readings from a particular pressure tap because each carried the same relative area-weighting. The 12

rakes were located radially over the compressor face 30° apart as diagrammed in figure 1(a). Six static pressure taps were mounted 60° apart along the circumference of the compressor case as shown in the same figure. Instrumentation of the compressor face also included four rakes of three thermocouples each mounted as shown in figure 1(b). Like the total-pressure taps just discussed, the thermocouples were mounted on the rakes in a fashion which provided each with the same relative area weighting.

The instrumentation between compressor stages included a rake of three total-pressure taps - one tap at the hub, one at the tip, and one at mid-span - such that their relative area-weightings were approximately 20, 20, and 60 percent, respectively. A similar rake of thermocouples was also mounted between each stage. Figure 1(c) is a diagram of the total-pressure and total-temperature instrumentation between compressor stages. Included in the figure is the corresponding instrumentation at the compressor discharge measuring station. Mean values of pressure and temperature at each measuring station throughout the compressor were obtained as area-weighted averages.

Engine airflow was obtained from static- and total-pressure measurements in the calibrated bellmouth inlet used in this experimental test program. The following well-known relations were applied:

$$\frac{P_t}{P_s} = \left[1 + \frac{\gamma - 1}{2} M^2\right]^{\gamma/(\gamma-1)} \tag{1}$$

$$\frac{\dot{W}\sqrt{\gamma g R T_t}}{C_d \gamma g P_t A} = \frac{M}{\left[1 + \frac{\gamma - 1}{2} M^2\right]^{(\gamma+1)/[2(\gamma-1)]}} \tag{2}$$

Given the total to static-pressure ratio in the bellmouth inlet duct, equation (1) can be solved for the corresponding Mach number M; it, in turn, can be used to evaluate the flow parameter expressed in equation (2).

Test Procedure

The steady-state compressor-inlet pressure and temperature for these tests were chosen to be 6.9 newtons per square centimeter and approximately 278 K, respectively. A steady-state engine operating condition with the maximum surge margin allowed by the reduced-area turbine diaphragm (232 cm^2) was established for the corrected rotor speed desired. When this operating point was established, the steady-state pressures and temperatures at all the instrumented measuring stations were recorded by a very

accurate data system called CADDE (ref. 9).

Next, a new operating point with less surge margin was established on the same speed line by reducing the exhaust nozzle area slightly while manually adjusting fuel flow to maintain constant corrected rotor speed. Again, the steady-state pressures and temperatures at all the instrumented measuring stations were recorded by CADDE. This procedure was continued until either compressor surge occurred or maximum temperature limits were reached. Corrected speed lines of 80, 87, 94, and 100 percent were established in this way for not only the clean compressor-inlet condition but also for the 14 distorted inlet-pressure conditions summarized in table I. (See fig. 2 for screens used to produce these distortions.)

The surge point for each corrected speed was determined by an extrapolation technique. In obtaining the experimental compressor map data, invariably the last set of steady-state data recorded by CADDE for each corrected speed was near, but not quite at, compressor surge. However, during the entire test procedure an operator monitored the turbine-discharge temperature on a gage in the test control room to determine when maximum temperature limits were being approached. As each CADDE point was being taken, the operator logged the corresponding turbine-discharge temperature. Likewise, the operator logged turbine-discharge temperature when compressor surge occurred. For each corrected speed, corrected airflow and overall compressor pressure ratio were mapped as functions of turbine-discharge temperature. These maps were then extrapolated to obtain the projected surge point for each corrected speed.

RESULTS AND DISCUSSION

The performance data presented in figures 3 to 6 are for the clean-inlet compressor with no distortion present, and the performance maps presented in figure 7 were obtained by exposing the compressor face to pressure distortions. These figures are presented in this report to add to the existing distortion data base. It should be noted that some of the previously published distortion data were obtained with engines whose inlet-guide-vane schedules were modified from the manufacturer's standard schedule (for instance, ref. 10). Therefore, one must exercise caution when trying to compare data from one set of engine tests with another. It is important to check that the critical engine operating conditions are the same before trying to compare the corresponding experimental data on a one-to-one basis, in order to avoid misrepresentations in the subsequent data analysis.

The experimental, clean compressor map and its extrapolated surge line are presented in figure 3. The 94-percent corrected speed line obtained in these tests exhibits unusual behavior as far as the shape of the curve is concerned. One would have ex-

pected the shape of the 94-percent corrected speed line to fit a smooth transition from low speed to high speed. This behavior has not been observed in experimental tests conducted in the past with other J85-13 engines.

The clean compressor was mapped on another occasion during this series of tests. The resulting 94-percent corrected speed line was identical to that obtained in the first mapping of the compressor. The phenomenon occurring at this speed was definitely repeatable and persisted throughout the entire experimental program. This unexpected result remains unexplained at this time. The fact that the interstage bleed valves were just full closed at 94-percent corrected speed seems to be coincidental and is being mentioned here just for the record.

Figure 4 presents for each compressor stage not only the experimental stage characteristic data points obtained in the current experimental tests but also the corresponding characteristic curve used in a digital simulation to model the current engine. The parameters displayed in figure 4 were obtained from equations of the form

$$\varphi_i = \frac{v_{z,i}}{\frac{2\pi N_*}{60} r_i} \tag{3}$$

$$\psi_i^P = \frac{K_i}{N_*^2} T_{i-1} \left[\left(\frac{P_i}{P_{i-1}} \right)^{(\gamma-1)/\gamma} - 1 \right] \tag{4}$$

where

$$K_i = \frac{\left(\frac{\gamma}{\gamma - 1} \right) gR}{\left(\frac{2\pi}{60} r_i \right)^2} \tag{5}$$

Moreover, $v_{z,i}$ satisfies the equation

$$\frac{\dot{W}_i \sqrt{\theta_{i-1}}}{A_i \delta_{i-1}} = \frac{v_{z,i}}{\sqrt{\theta_{i-1}}} \left[1 - \left(\frac{v_{z,i}}{\sqrt{\theta_{i-1}}} \right)^2 \frac{1}{2g_* J c_p T_0 \cos^2 \beta_i} \right]^{1/(\gamma-1)} \rho_0 \tag{6}$$

derived in appendix B of reference 5. The tip-radius of the i^{th} compressor stage r_i

has the value 20.19 centimeters when $i = 1$, 19.80 centimeters when $i = 2$, and 19.69 centimeters otherwise. The absolute air angle at the rotor inlet β_i and the effective area A_i of each compressor stage are presented in table II.

Equation (6) may be used to solve iteratively for $v_{z,i}/\sqrt{\theta_{i-1}}$ as a function of $\dot{W}_i \sqrt{\theta_{i-1}}/(A_i \delta_{i-1})$. However, for the range of the experimental data covered in these tests the relationship between the parameters $v_{z,i}/\sqrt{\theta_{i-1}}$ and $\dot{W}_i \sqrt{\theta_{i-1}}/(A_i \delta_{i-1})$ in equation (6) is approximately second order. Second-order least-squares curve fits of the experimental data resulted in accuracy to within 0.5 percent. For convenience, these curve fits are included in table III for each compressor stage.

An experimental characteristic data point for each compressor stage was obtained at each operating point for which a CADDE point was taken in mapping the clean-inlet compressor. Each of the CADDE points provided values of engine airflow and average pressure and temperature for every compressor stage; hence, equations (3) and (4) could be evaluated at each experimental CADDE point taken.

In mapping the clean-inlet compressor, CADDE points were taken for each corrected speed over the maximum range of pressure ratio and corrected airflow allowed by the smaller size turbine diaphragm. Thus, the experimental data points shown in figure 4 represent the full operating range of this experimental engine configuration. However, the experimental data cover a rather limited range which complicates the problem of determining suitable maps with sufficiently broad range to be incorporated in a simulation of the engine. The stage characteristic curves used by Willoh and Seldner in their analog simulation were based primarily on manufacturer's data (derived from wall static-pressure measurements on a development engine). Curves of the same basic shapes were used with the current experimental data but were adjusted where necessary to fit the data and yield an overall compressor map that was in good agreement with the experimental engine data.

As previously mentioned, the inlet guide vanes on the J85-13 engine are mechanically linked to the interstage bleeds so that both parts of the system operate together at a uniform rate. For the tests reported here the bleeds were fully open when the inlet guide vanes were cambered at their maximum angle; they were fully closed when the inlet-guide-vane position was axial. The experimental data in figure 4(a) shows that the position of the inlet guide vanes has a significant effect on the performance characteristics of the first compressor stage. Hence, stage 1 is modeled using three separate characteristic curves for the simulation: one for conditions corresponding to the inlet guide vanes fully cambered ($N_c \leq 80$ %), one for the inlet guide vanes positioned at midtravel ($N_c = 87$ %), and one for the inlet guide vanes positioned axially ($N_c \geq 94$ %). Characteristic values for conditions corresponding to other intermediate inlet-guide-vane positions can be obtained in a digital simulation by using the very efficient interpolation scheme discussed in reference 11. The cluster of data points that are low in

stage 2 (solid points in fig. 4(b)) correspond to a corrected speed of 100 percent as does the cluster of points that are high in stage 3 (solid points in fig. 4(c)). The experimental stage characteristic data obtained for stages 2 and 3 suggest that an experimental value obtained at the measuring station between these stages was not representative of the mean parameter value. In particular, the fact that pressure ratio across stage 2 is low and that across stage 3 is high suggests that the measured discharge pressure from stage 2 is low at a corrected speed of 100 percent. Accordingly, the levels of the characteristic curves for these two stages were set on the basis of the data from the other corrected speeds.

The analog model developed by Willoh and Seldner has also been programmed on the digital computer. In addition to the curves relating the pressure coefficient ψ_i^P to the flow coefficient φ_i, another set of curves required by the simulation are those relating efficiency η_i to the flow coefficient φ_i. The nature of the equation

$$\eta_i = \frac{\left(\frac{P_i}{P_{i-1}}\right)^{(\gamma-1)/\gamma} - 1}{\frac{T_i}{T_{i-1}} - 1} \tag{7}$$

is such that small variations in the measured values of the experimental temperature and pressure become amplified, aggravating the scatter in the efficiency parameter η_i. Thus, the resultant experimental data band on a graph of efficiency η_i versus flow coefficient φ_i can mask the level at which efficiency should be set. The stage efficiency curves were not changed from those used to digitally represent the analog model of Willoh and Seldner. For the convenience of the reader the efficiency curves used are presented in figure 5.

Figure 6 presents the compressor map obtained by including in the digital simulation the new stage characteristic maps previously discussed. In this figure the simulation undistorted compressor map is also compared with the corresponding experimental compressor map from the data base. The 80-, 87-, and 100-percent corrected speed lines agree very well with the corresponding experimental data. The maximum deviation from the experimental data for these three speed lines occurs at 87 percent corrected speed at a pressure ratio of about 5.0. The error in corrected airflow there is approximately 1.1 percent. The shape of the simulation 94-percent corrected speed line looks more like what one would expect from the experimental engine at this speed if the speed line is compared with the 87 and 100 percent curves. However, none of the attempts to try to match both the 94- and 100-percent experimental corrected speed lines in the digital simulation were successful. The inlet-guide-vane position is the

same at each of these corrected speeds and any adjustment attempted in the simulation that helped the one speed line hindered the other. However, because a choice had to be made it seemed more important to match the experimental 100-percent corrected speed line as closely as possible. Not only is this military speed for the J85-13 engine; but, more important, the shape of the 94-percent corrected speed line is suspect to begin with.

Figure 7 presents the compressor data resulting from exposing the compressor inlet to 14 different distortion patterns. Distortions in total pressure were introduced at the compressor face by means of screens mounted in the inlet duct approximately one duct diameter upstream of the compressor face. However, the experimental test procedure was identical to that previously described for the clean-inlet compressor.

Table I presents a summary of the distorted-inlet conditions run. Ten circumferential patterns and four radial patterns were tested. If the distortion screen covered a sector of the compressor face, the test condition is designated as a circumferential distortion pattern, and its angle of extent is defined to be equal to the central angle subtended by the distortion screen. However, if the distortion screen covered a ring of the compressor face, the test condition is designated a radial distortion pattern. A radial distortion located at the hub or tip of the compressor face is referred to as a hub-radial or tip-radial pattern, respectively. Also, the term "distortion screen density" is used to designate the percent of area blocked by the screen wire per unit area of screen. As can be seen from the pressure drop characteristics presented in table IV, the pressure ratio across a particular distortion screen decreases as corrected speed increases. In addition, examples of circumferential, hub-radial, and tip-radial distortion patterns are presented in figure 2.

The angle of extent of the circumferential distortion patterns ranged from 30° to 180°, and the distortion screen density varied from 26 to 69 percent, while the hub-radial and tip-radial distortion patterns spoiled 40 percent of the compressor face area with distortion screen densities of 42 and 49 percent, respectively. Pressure ratio $\overline{P}_3/\overline{P}_2$ as shown in figure 7 is the mean pressure measured at compressor discharge normalized to the mean pressure measured at the compressor face. Airflow $\dot{W}$ is the mean flow of air through the calibrated bellmouth inlet, and corrected airflow $\dot{W}_c$ is airflow corrected to the mean compressor-face pressure and temperature conditions.

The figures present the experimental data points taken for each distortion pattern superimposed on the clean-inlet compressor map. No experimental data are shown at 100 percent corrected speed in figure 7(a) because compressor surge occurred trying to establish an operating point at that speed. Except for four speeds at which temperature limits were reached before compressor surge occurred (see figs. 7(a), 7(i), 7(j)), the figures also include the extrapolated surge point for each corrected speed obtained using the technique previously discussed. Examining the experimental distortion data,

one can make the general observation that the largest variance from the clean-inlet compressor map occurs at the higher corrected speeds. The data at the lower corrected speeds generally agree with the clean-inlet speed lines better than do the higher speeds. They also maintain the shapes of the clean-inlet speed lines even though they are sometimes shifted from them.

SUMMARY OF RESULTS

A General Electric J85-13 engine was used in a recent series of experimental tests at the Lewis Research Center. Each of the eight compressor stages was instrumented to obtain the characteristics of the individual stages. Individual stage modeling is required to study dynamic distortion or to predict compressor surge for both steady-state and dynamic distortion.

Presented in this report are the experimental compressor stage characteristics and the resulting stage map representations. These maps were included in a stage-by-stage simulation of the engine, and the resulting clean-inlet compressor map was compared with the corresponding experimental map. The two were in very good agreement at corrected speeds of 80, 87, and 100 percent. The maximum deviation from the experimental data for these three speed lines occurred at 87 percent corrected speed at a pressure ratio of about 5.0. The error in corrected airflow there was approximately 1.1 percent.

In addition, subsequent tests in this series introduced 14 distortion patterns at the face of the compressor using screens of varying densities and patterns. The study included 10 circumferential and 4 radial distortion patterns each with a spoiled area which ranged from 8 to 50 percent of the compressor-face total area. The density of the distortion screen varied from 26 to 69 percent. In general, the largest variance from the clean-inlet compressor map occurs at the higher corrected speeds. At the lower corrected speeds the shapes of the clean-inlet speed lines are maintained even though the data are sometimes shifted from them. These performance data are included in this report to complete a data base that may be used in further investigations of the effects of inlet distortion on compressor performance and stability.

Lewis Research Center,
National Aeronautics and Space Administration,
Cleveland, Ohio, July 23, 1975,
505-05.

APPENDIX - SYMBOLS

A	area, m^2
a_0	curve fit coefficient, m/sec
a_1	curve fit coefficient, m^3/kg
a_2	curve fit coefficient, $(m^5 \cdot sec)/kg^2$
C_d	flow coefficient
c_p	specific heat at constant pressure, $J/(kg \cdot K)$
g	gravitational constant, 9.81 m/sec^2
g_*	gravitational conversion factor, 1 $(kg \cdot m)/(N \cdot sec^2)$
J	mechanical equivalent of heat, 1 $(N \cdot m)/J$
M	Mach number
N	percent of rated engine speed (16 500 rpm)
N_*	rotational speed, rpm
P	pressure, N/m^2
P_i	total pressure at i^{th} compressor stage measuring station, N/m^2
$\overline{P}_2$	mean total pressure at compressor inlet measuring station, N/m^2
$\overline{P}_3$	mean total pressure at compressor discharge measuring station, N/m^2
R	universal gas constant, 29.2 m/K
r	tip radius, m
ss	inlet-guide-vane angle, deg
T	temperature, K
T_i	total temperature at i^{th} compressor stage measuring station, K
v_z	axial velocity, m/sec
$\dot{W}$	mass flow, kg/sec
β	absolute air angle at rotor inlet, deg
γ	ratio of specific heats, 1.4
δ	ratio of total pressure to standard atmospheric pressure
η	efficiency
θ	ratio of total temperature to standard atmospheric temperature

ρ mass density, kg/m^3

φ flow coefficient

ψ^P pressure coefficient

Subscripts:

c corrected

i number designating the i^{th} compressor stage

s static condition

t total condition

0 standard atmospheric condition

REFERENCES

1. Calogeras, James E.: Experimental Investigation of Dynamic Distortion in a Mach 2.50 Inlet with 60 Percent Internal Contraction and its Effect on Turbojet Stall Margin. NASA TM X-1842, 1969.

2. Werner, Roger A.; Abdelwahab, Mahmood; and Braithwaite, Willis M.: Performance and Stall Limits of an Afterburner-Equipped Turbofan Engine with and without Inlet Flow Distortion. NASA TM X-1947, 1970.

3. Braithwaite, Willis M.; Graber, Edwin J., Jr.; and Mehalic, Charles M.: The Effects of Inlet Temperature and Pressure Distortion on Turbojet Performance. Presented at the 9th Propulsion Joint Specialists Conf., Las Vegas, Nev., Nov. 5-7, 1973. (Also NASA TM X-71431.)

4. Burstadt, Paul L.; and Calogeras, James E.: Instantaneous Distortion in a Mach 2.5, 40-Percent-Internal-Contraction Inlet and its Effect on Turbojet Stall Margin. NASA TM X-3002, 1974.

5. Willoh, Ross G.; and Seldner, Kurt: Multistage Compressor Simulation Applied to the Prediction of Axial Flow Instabilities. NASA TM X-1880, 1969.

6. Seldner, Kurt; Mihaloew, James R.; and Blaha, Ronald J.: Generalized Simulation Technique for Turbojet Engine System Analysis. NASA TN D-6610, 1972.

7. Daniele, Carl J.; Blaha, Ronald J.; and Seldner, Kurt: Prediction of Axial Flow Instabilities in a Turbojet Engine by Use of a Multistage Compressor Simulation on the Digital Computer. NASA TM X-3134, 1975.

8. Wenzel, Leon M.; Moss, John E., Jr.; and Mehalic, Charles M.: Effect of Casing Treatment on the Performance of a Multistage Compressor. NASA TM X-3175, 1975.

9. Mealey, Charles; and Kee, Leslie: A Computer-Controlled Central Digital Data Acquisition System. NASA TN D-3904, 1967.

10. Calogeras, James E.; Johnsen, Roy L.; and Burstadt, Paul L.: Effect of Screen-Induced Total-Pressure Distortion on Axial-Flow Compressor Stability. NASA TM X-3017, 1974.

11. Hart, Clint E.: Function Generation Subprograms for Use in Digital Simulations. NASA TM X-71526, 1974.

TABLE I. - SUMMARY OF SCREEN PATTERNS USED IN DISTORTION TESTS

Type of distortion	Angle of extent, deg	Spoiled-area ratio, percent	Distortion screen density, percent	Figure
Circumferential	60	$16\frac{2}{3}$	69	7(a)
	180	50	49	7(b)
	90	25	49	7(c)
	60	$16\frac{2}{3}$	49	7(d)
	180	50	42	7(e)
	90	25	↓	7(f)
	60	$16\frac{2}{3}$		7(g)
	30	$8\frac{1}{3}$		7(h)
	180	50	26	7(i)
	90	25	26	7(j)
Hub-radial	360	40	49	7(k)
			42	7(l)
Tip-radial	360	40	49	7(m)
			42	7(n)

TABLE II. - ABSOLUTE AIR ANGLE AT ROTOR INLET AND EFFECTIVE AREA FOR EACH COMPRESSOR STAGE

Compressor stage	Absolute air angle at rotor inlet, deg	Effective area, cm^2
1	(a)	960.6
2	5.4	756.5
3	12.1	614.7
4	14.8	506.6
5	19.4	422.7
6	23.2	365.5
7	22.2	333.2
8	21.6	322.7

[a] $\beta_1 = \frac{ss}{3}(1.85 - 0.01\ ss)$ where $ss = 33$ for $N_c \leq 80$, $ss = 33/14\ (94 - N_c)$ for $80 < N_c < 94$, and $ss = 0$ for $N_c \geq 94$.

TABLE III. - SECOND-ORDER LEAST SQUARES CURVE

FIT OF $\frac{v_{z,i}}{\sqrt{\theta_{i-1}}}$ AS FUNCTION OF $\frac{\dot{W}_i \sqrt{\theta_{i-1}}}{A_i \delta_{i-1}}$

$$\left[\text{Form: } \frac{v_{z,i}}{\sqrt{\theta_{i-1}}} = a_0 + a_1\left(\frac{\dot{W}_i \sqrt{\theta_{i-1}}}{A_i \delta_{i-1}}\right) + a_2\left(\frac{\dot{W}_i \sqrt{\theta_{i-1}}}{A_i \delta_{i-1}}\right)^2\right]$$

Stage	a_0, m/sec	a_1, m^3/kg	a_2, $(m^5 \cdot sec)/kg^2$
1	74.92	-0.2387	0.004155
2	74.37	-.2324	.004140
3	68.28	-.1755	.004049
4	42.81	.1342	.003124
5	15.25	.4846	.002041
6	20.32	.4106	.002342
7	21.09	.4013	.002356
8	7.85	.6262	.001412

TABLE IV. - DISTORTION SCREEN CHARACTERISTICS

AT MAXIMUM ANGLE OF EXTENT

Screen density, percent	Mean corrected speed, percent of rated	Mean pressure ratio across screen
26	80.0	0.978
	87.1	.970
	94.2	.961
	100.0	.947
42	80.1	0.959
	87.1	.942
	94.0	.925
	100.1	.894
49	80.0	0.950
	87.0	.930
	94.0	.907
	100.1	.870
69	80.0	0.926
	87.1	.898
	94.1	.868

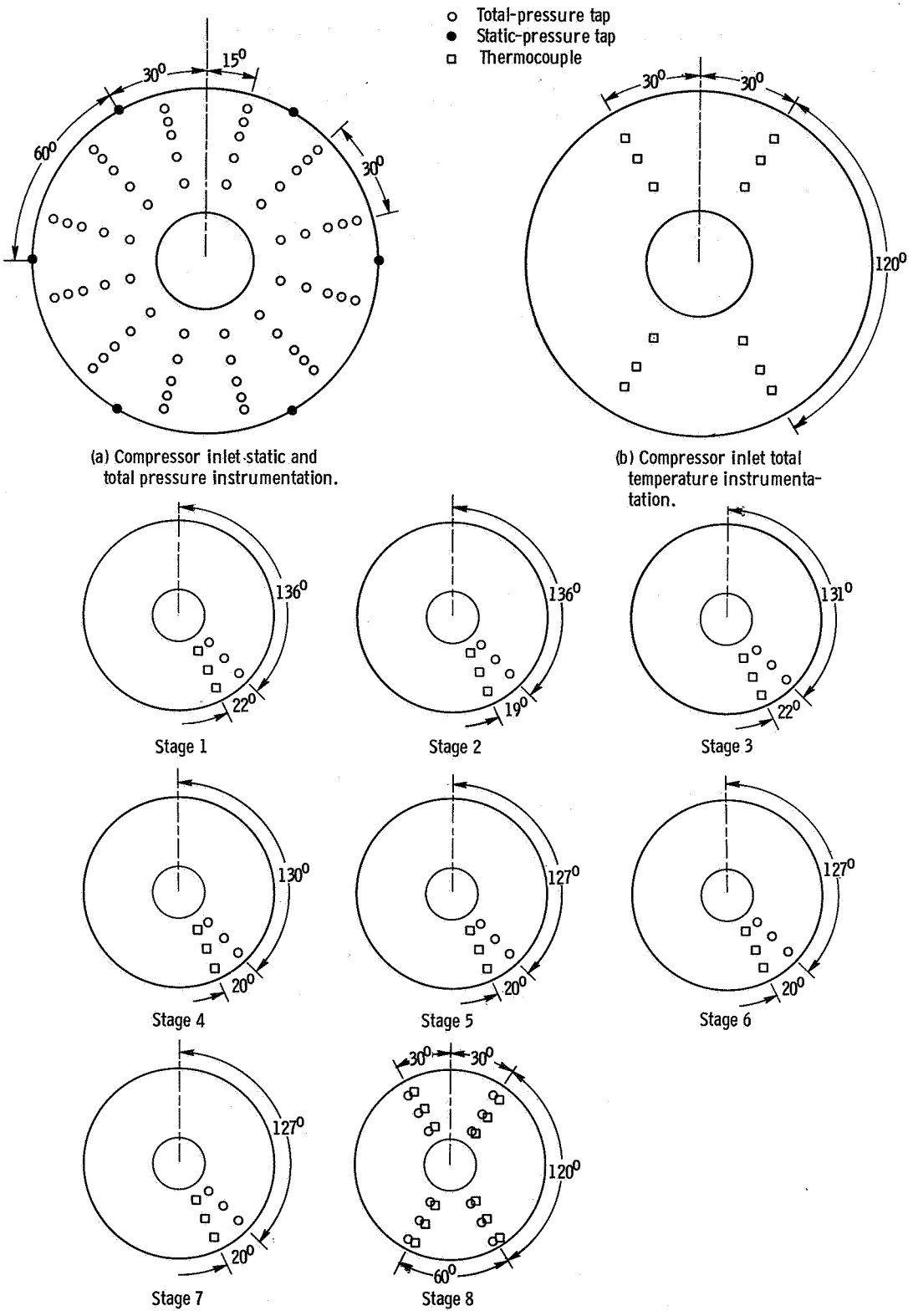

(a) Compressor inlet static and total pressure instrumentation.

(b) Compressor inlet total temperature instrumentation.

(c) Compressor stage discharge measuring stations (looking upstream).

Figure 1. - Compressor inlet and stage instrumentation.

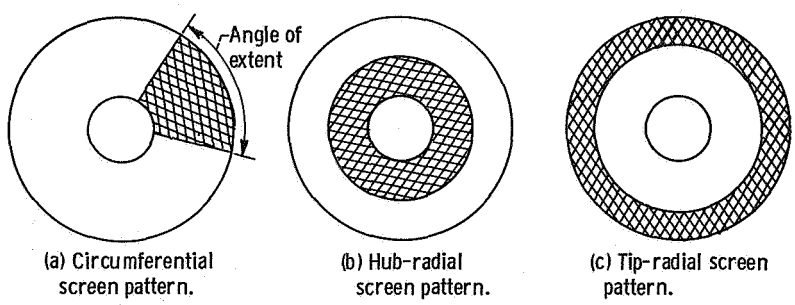

Figure 2. - Screen patterns used to induce inlet pressure distortion.

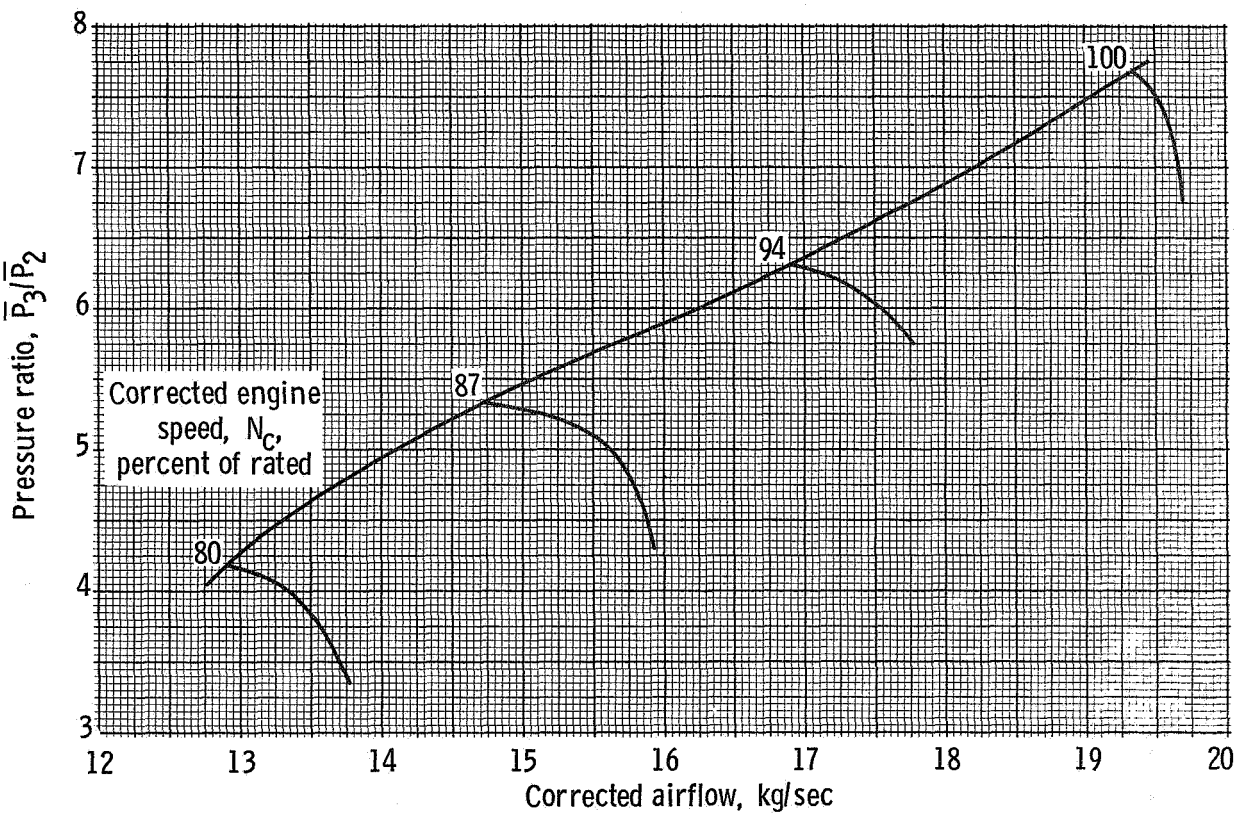

Figure 3. - Experimental compressor map with extrapolated surge line.

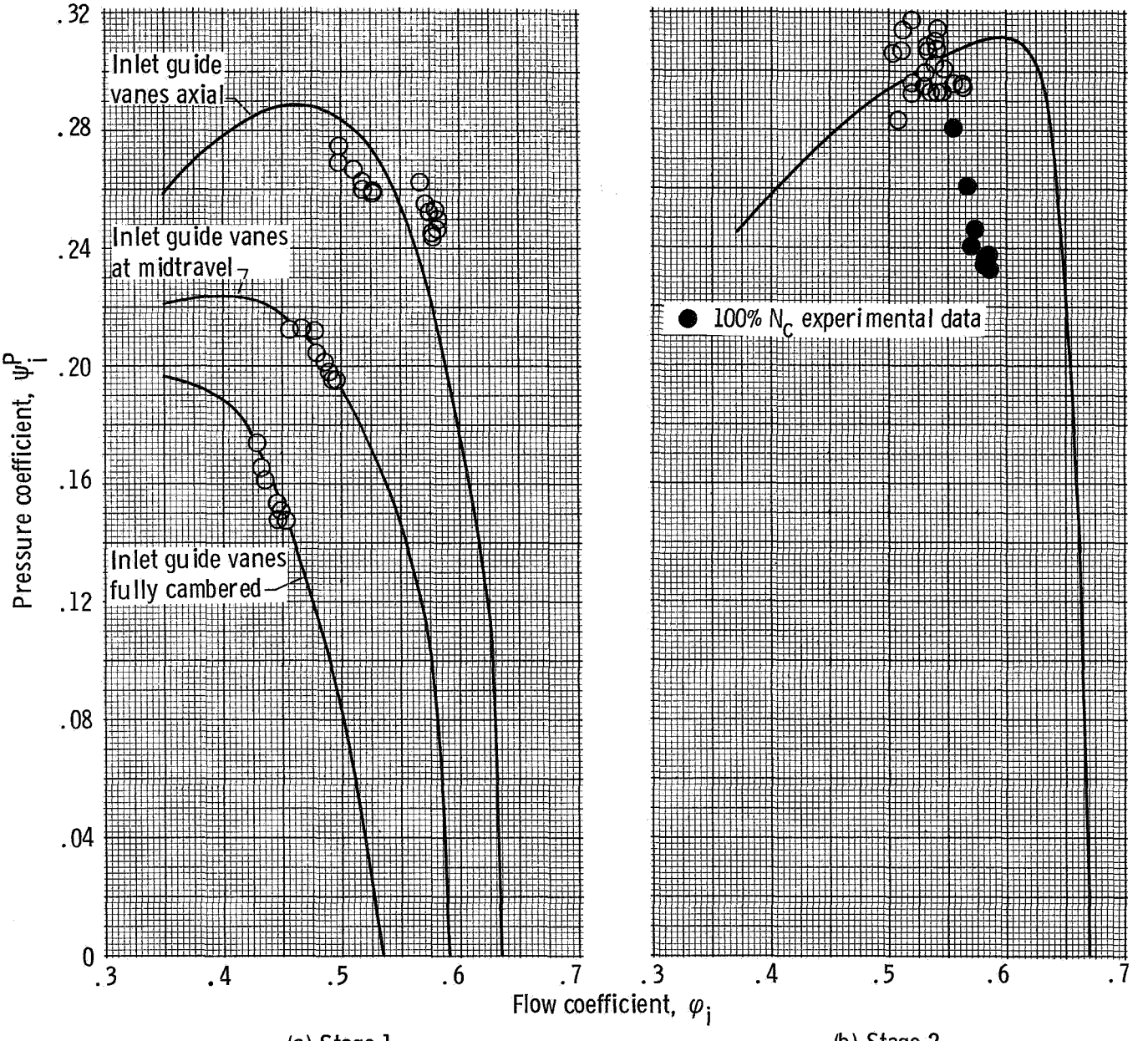

(a) Stage 1.

(b) Stage 2.

Figure 4. - Compressor stage characteristics used in simulation model together with corresponding experimental data points. (Subscript i denotes stage number.)

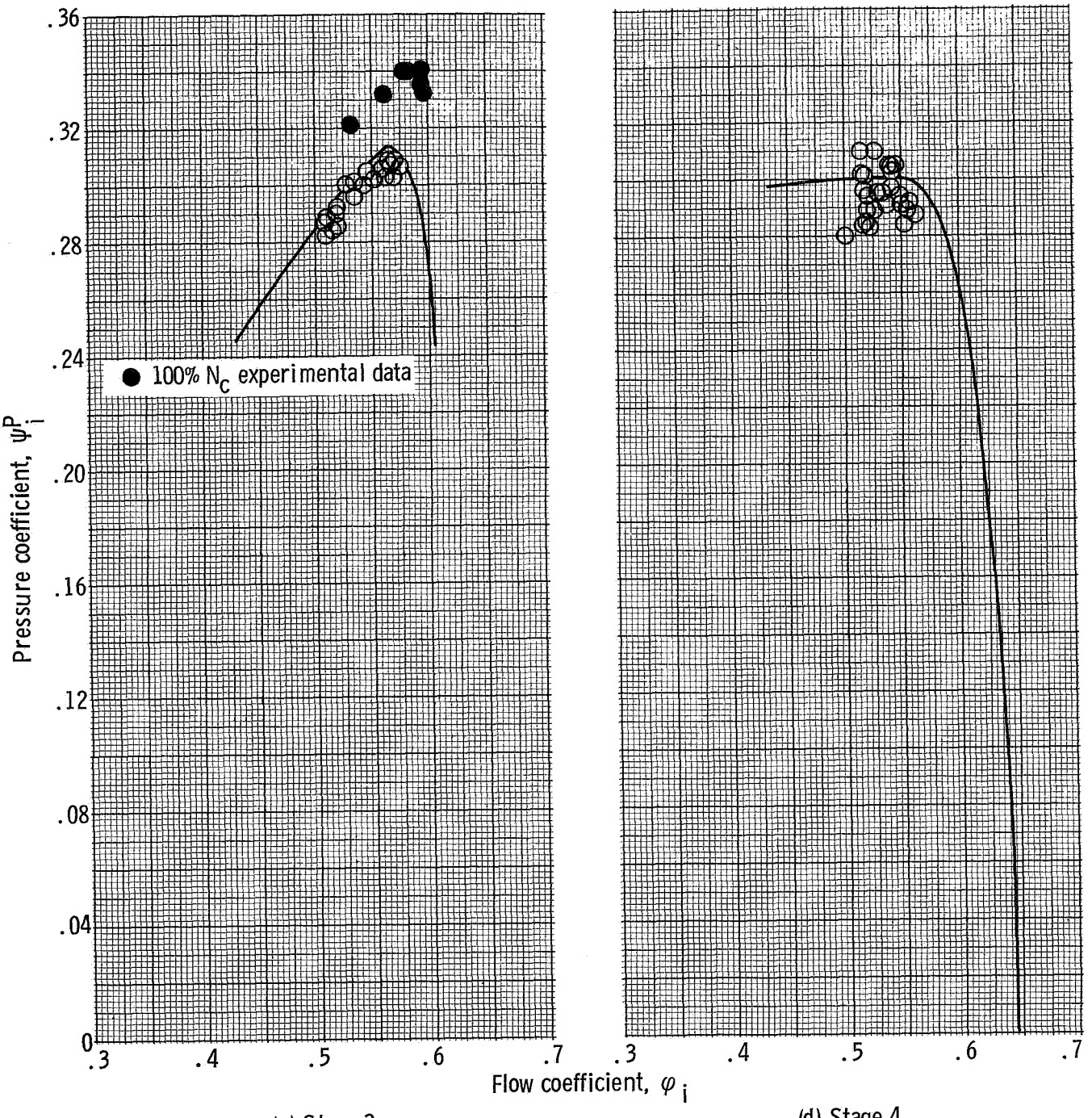

(c) Stage 3.

(d) Stage 4.

Figure 4. - Continued.

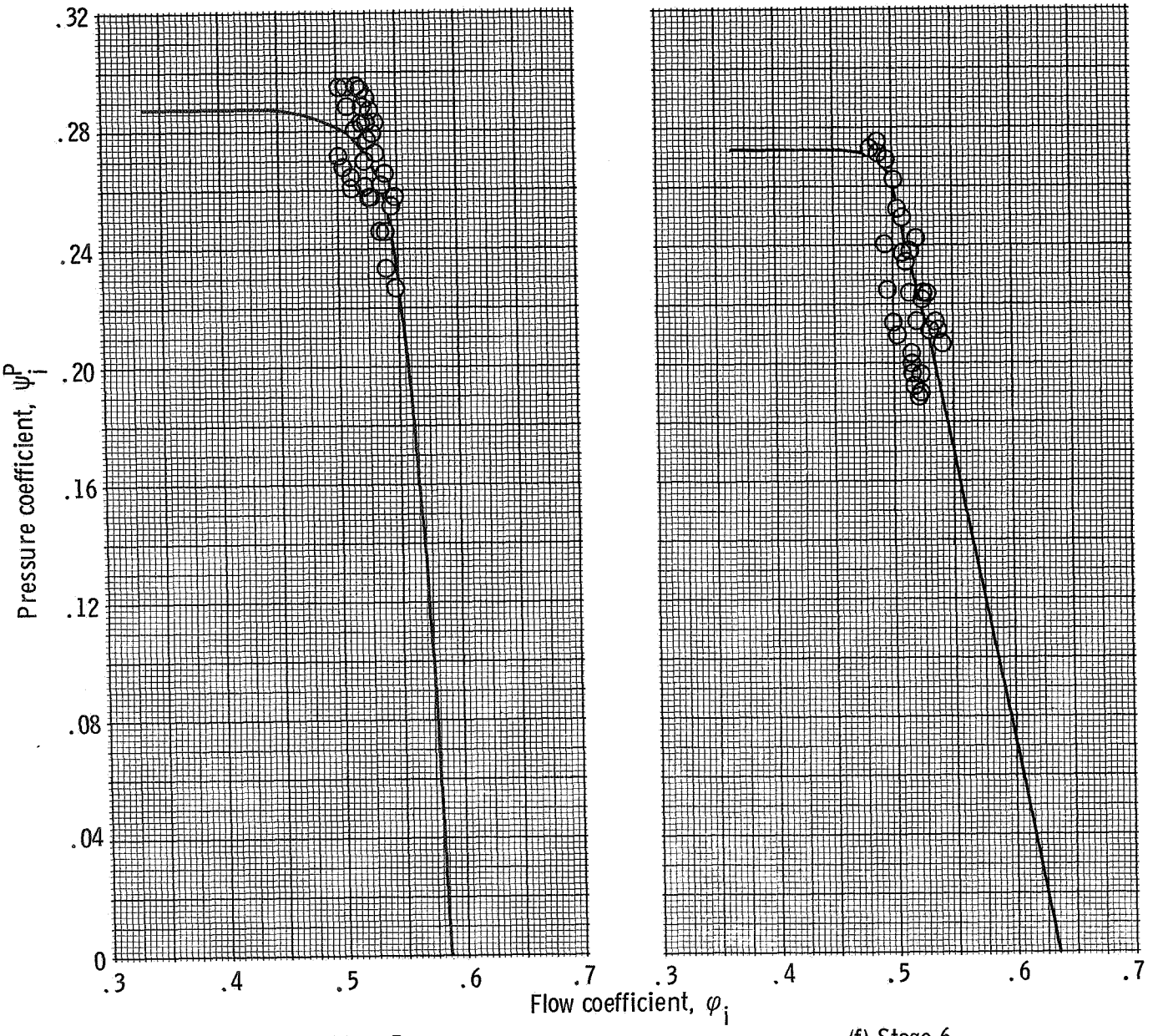

(e) Stage 5.

(f) Stage 6.

Figure 4. - Continued.

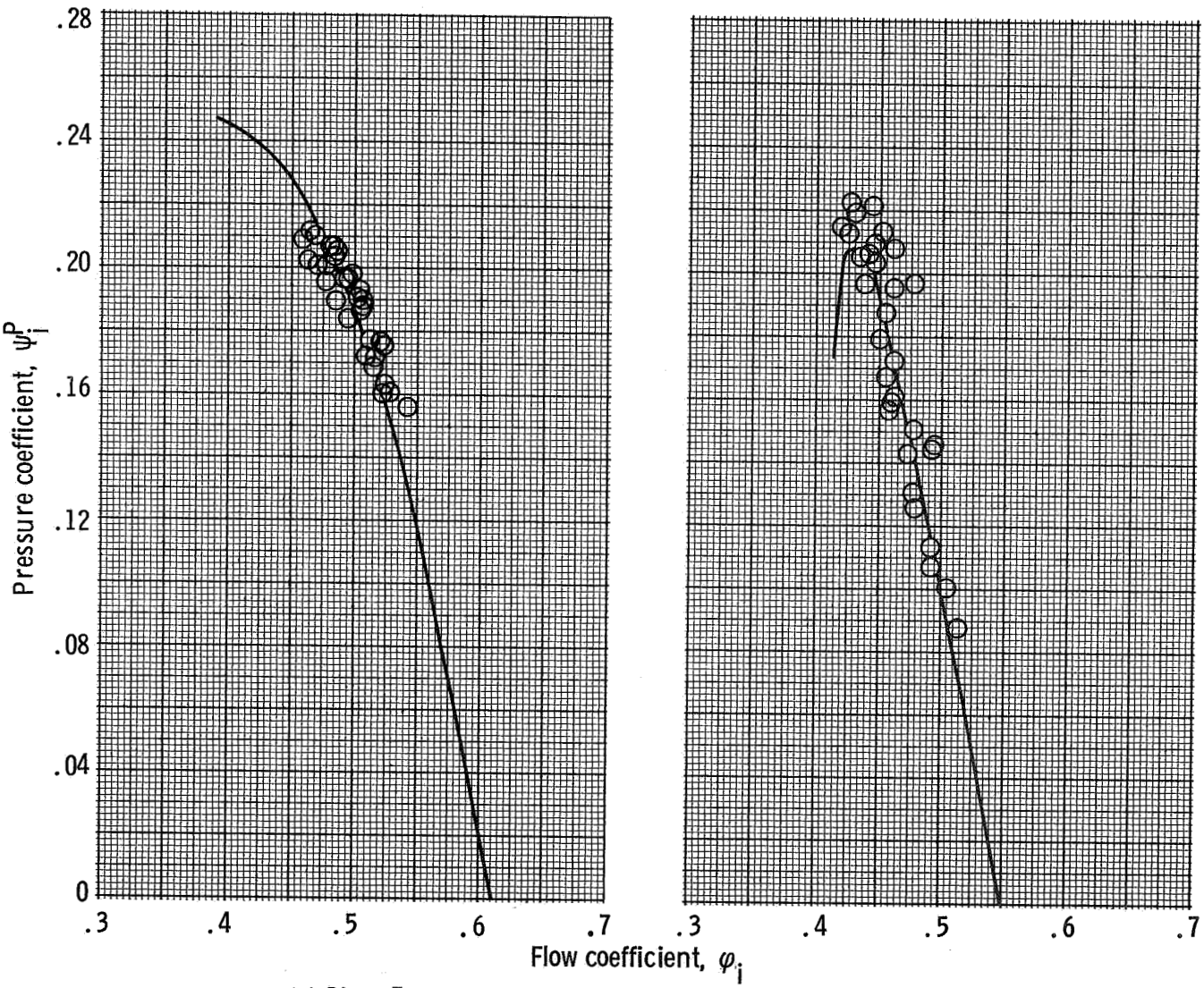

(g) Stage 7.

(h) Stage 8.

Figure 4. - Concluded.

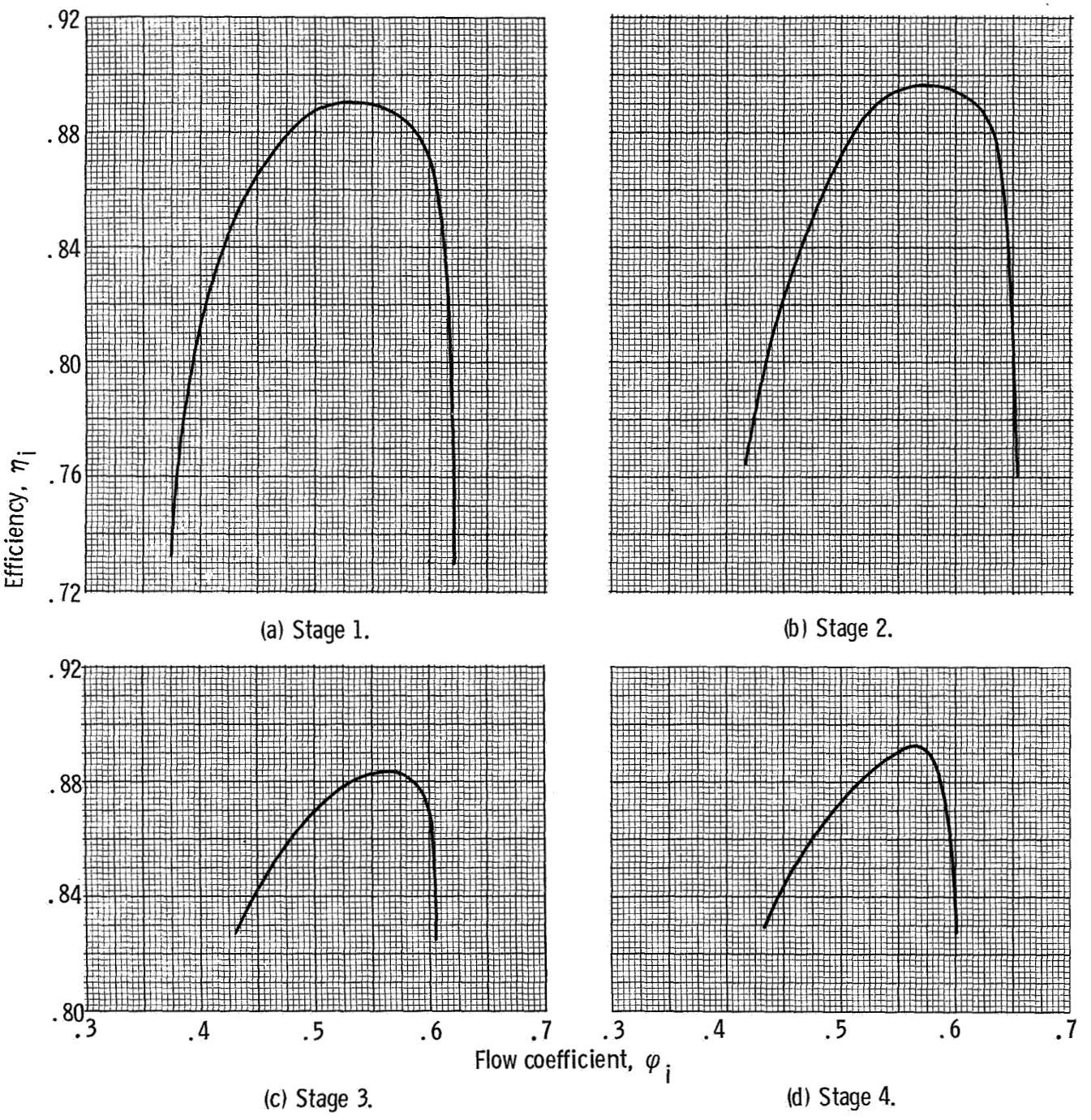

Figure 5. - Compressor stage efficiency curves used in simulation model. (Subscript i denotes stage number.)

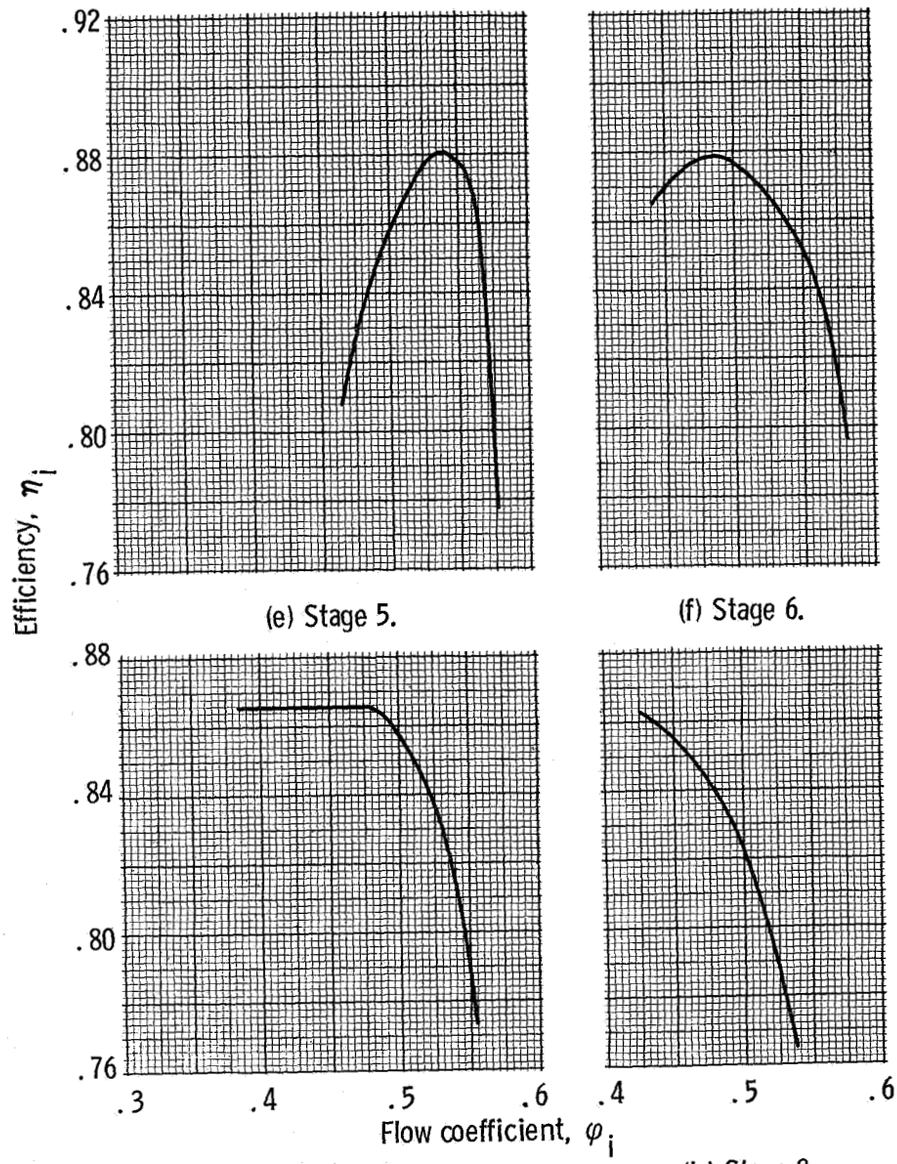

Figure 5. - Concluded.

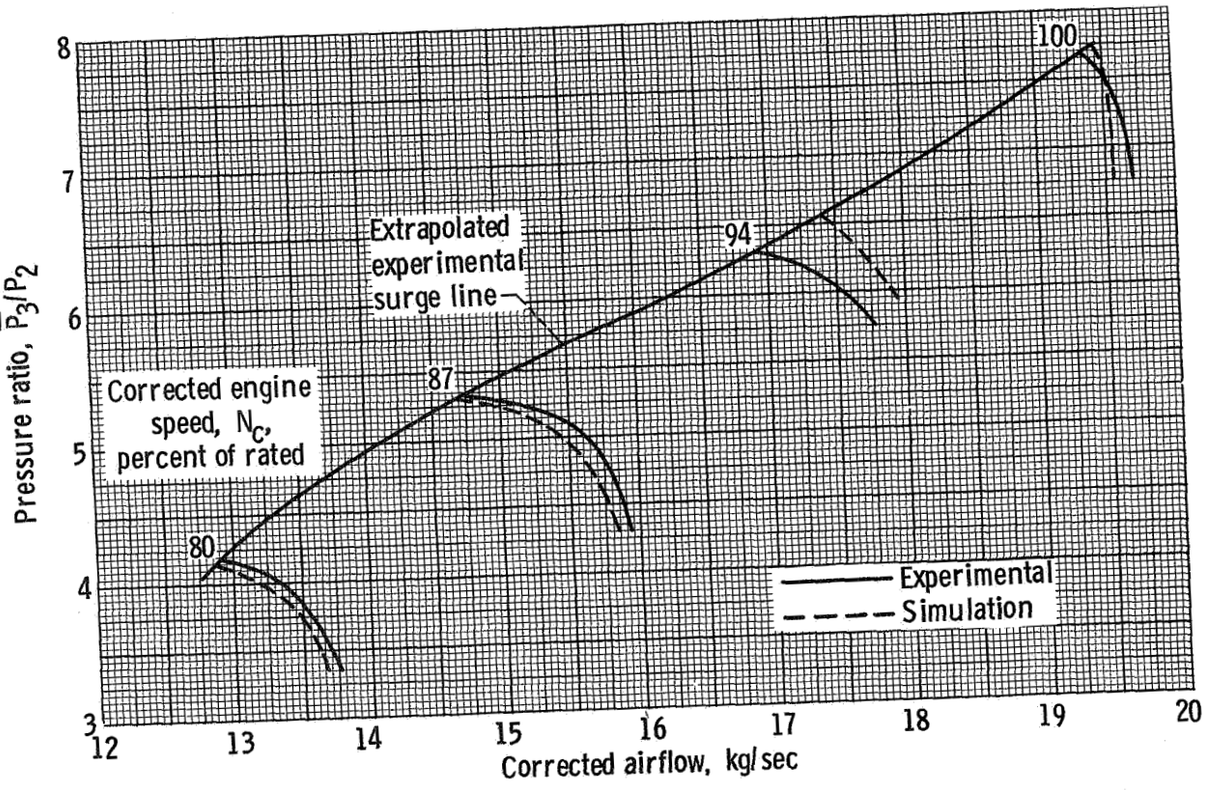

Figure 6. - Comparison of analytical compressor and experimental compressor maps for clean inlet.

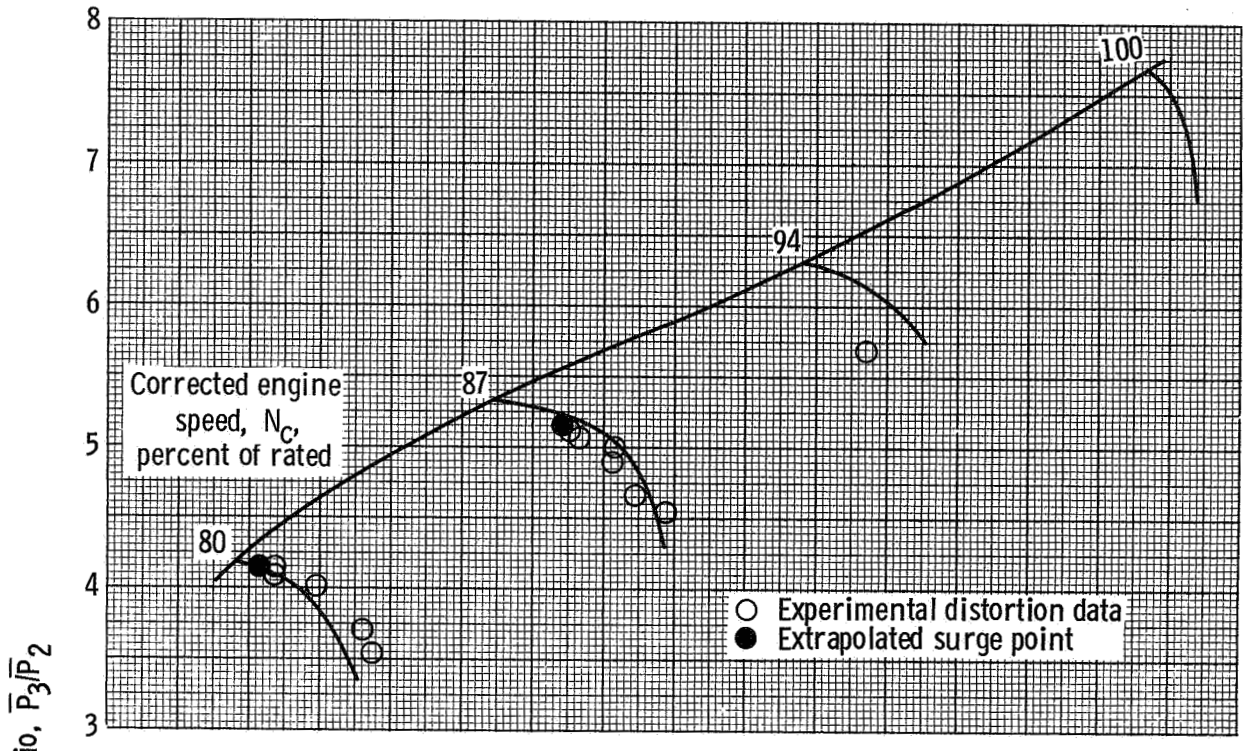

(a) Circumferential distortion; angle of extent, 60^0; distortion screen density, 69 percent.

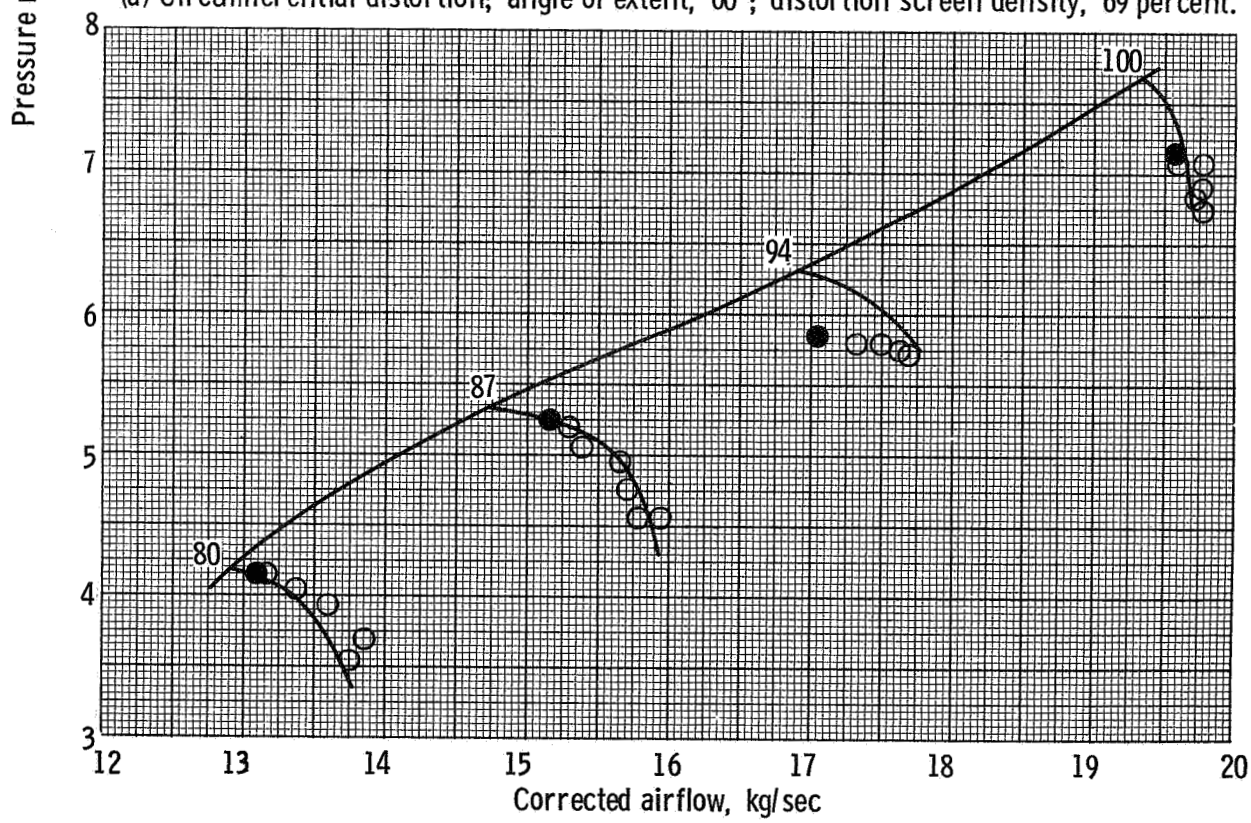

(b) Circumferential distortion; angle of extent, 180^0; distortion screen density, 49 percent.

Figure 7. - Clean experimental compressor map with extrapolated surge line showing experimental data points for various distortion patterns.

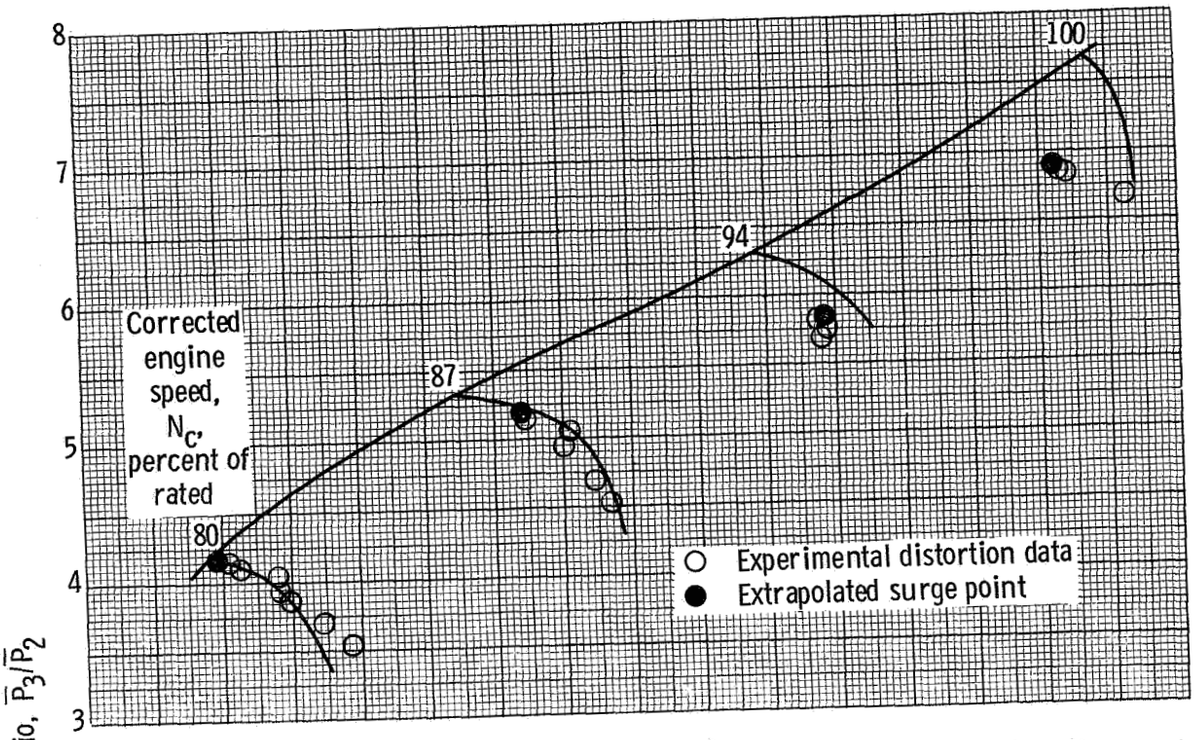

(c) Circumferential distortion; angle of extent, 90^0; distortion screen density, 49 percent.

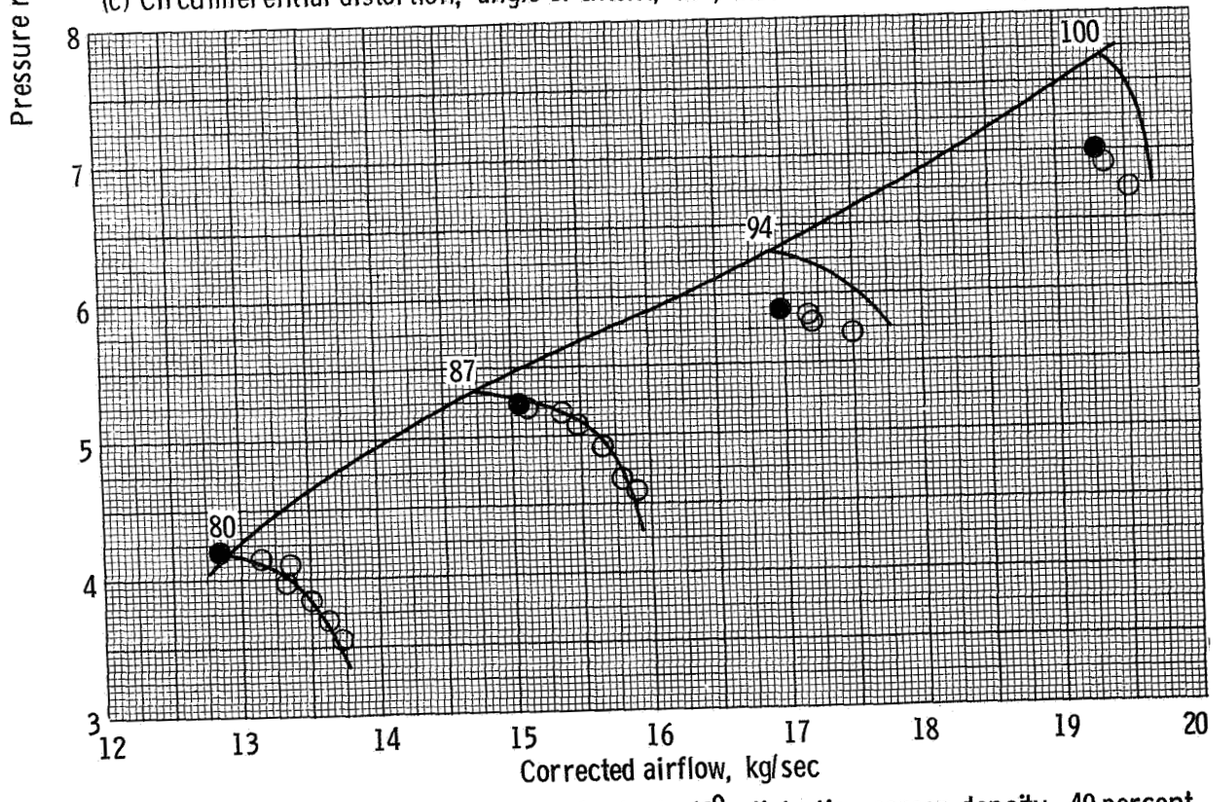

(d)Circumferential distortion; angle of extent, 60^0; distortion screen density, 49 percent.

Figure 7. - Continued.

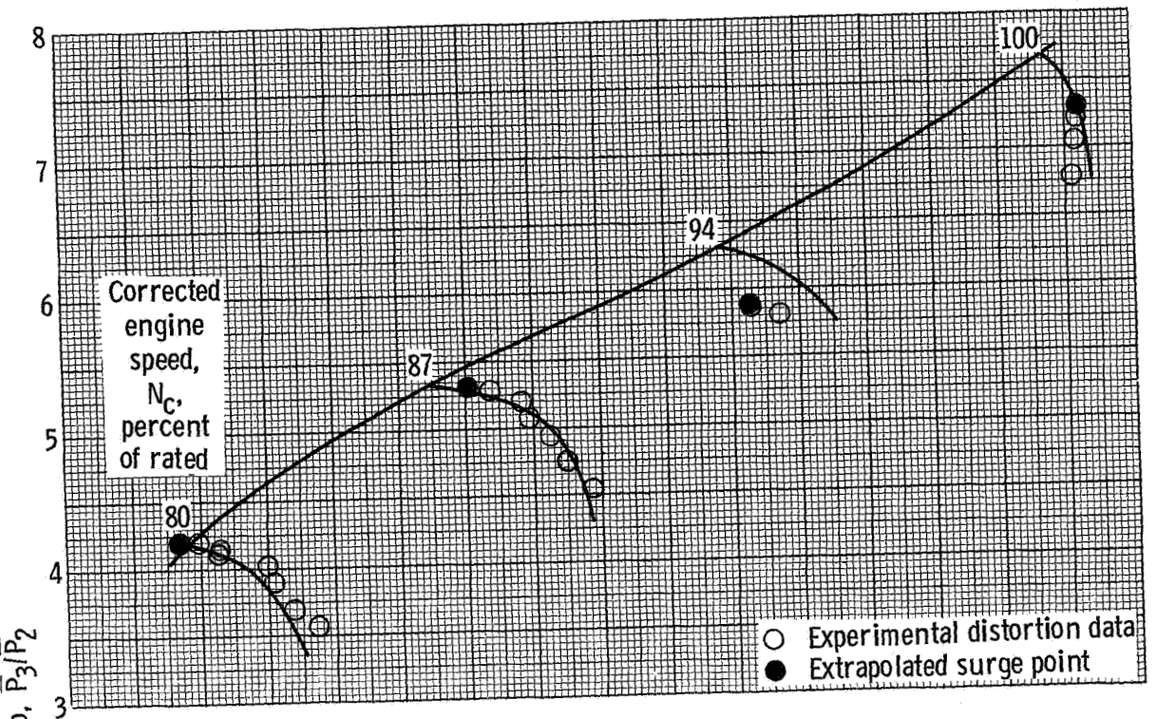

(e) Circumferential distortion; angle of extent, 180°; distortion screen density, 42 percent.

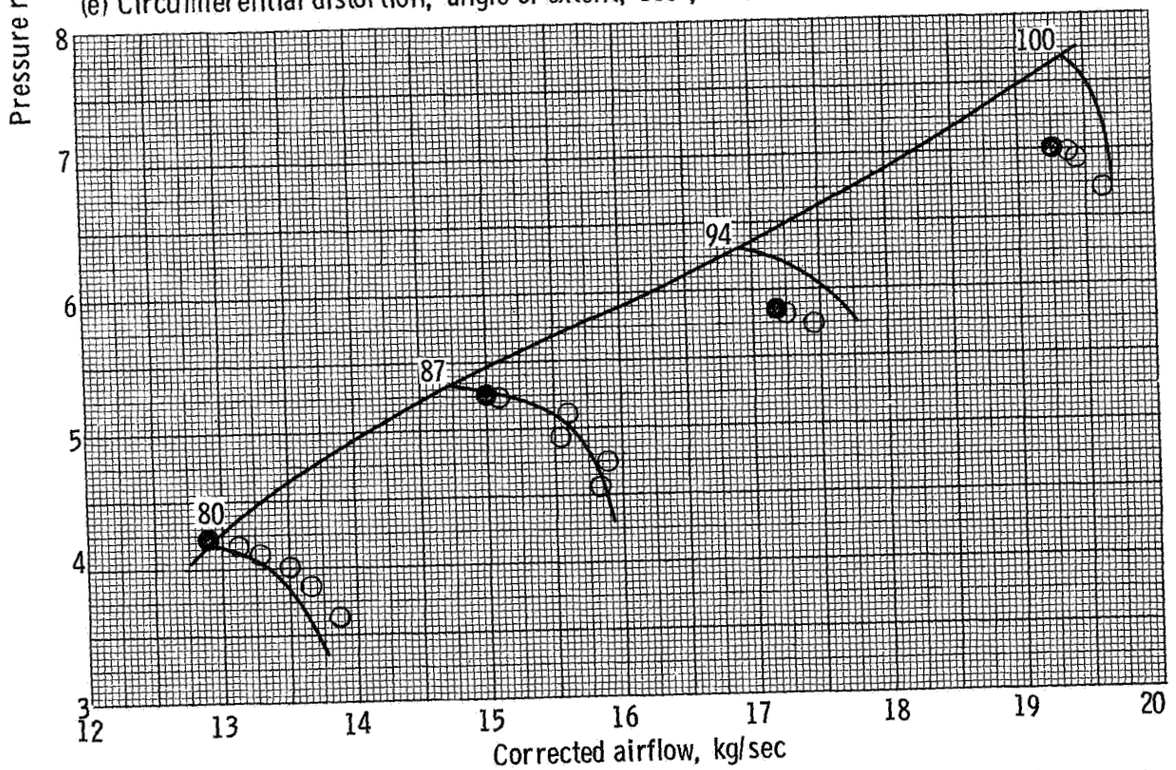

(f) Circumferential distortion; angle of extent, 90°; distortion screen density, 42 percent.

Figure 7. - Continued.

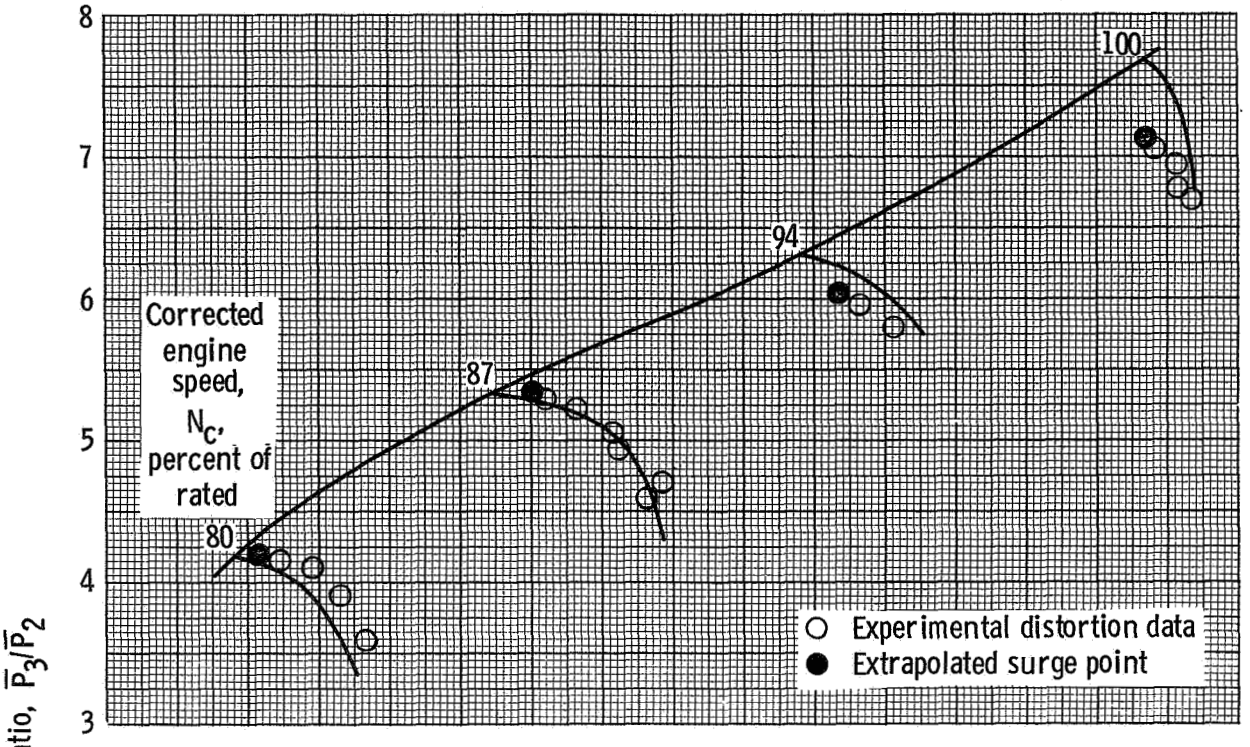

(g) Circumferential distortion; angle of extent, 60^0; distortion screen density, 42 percent.

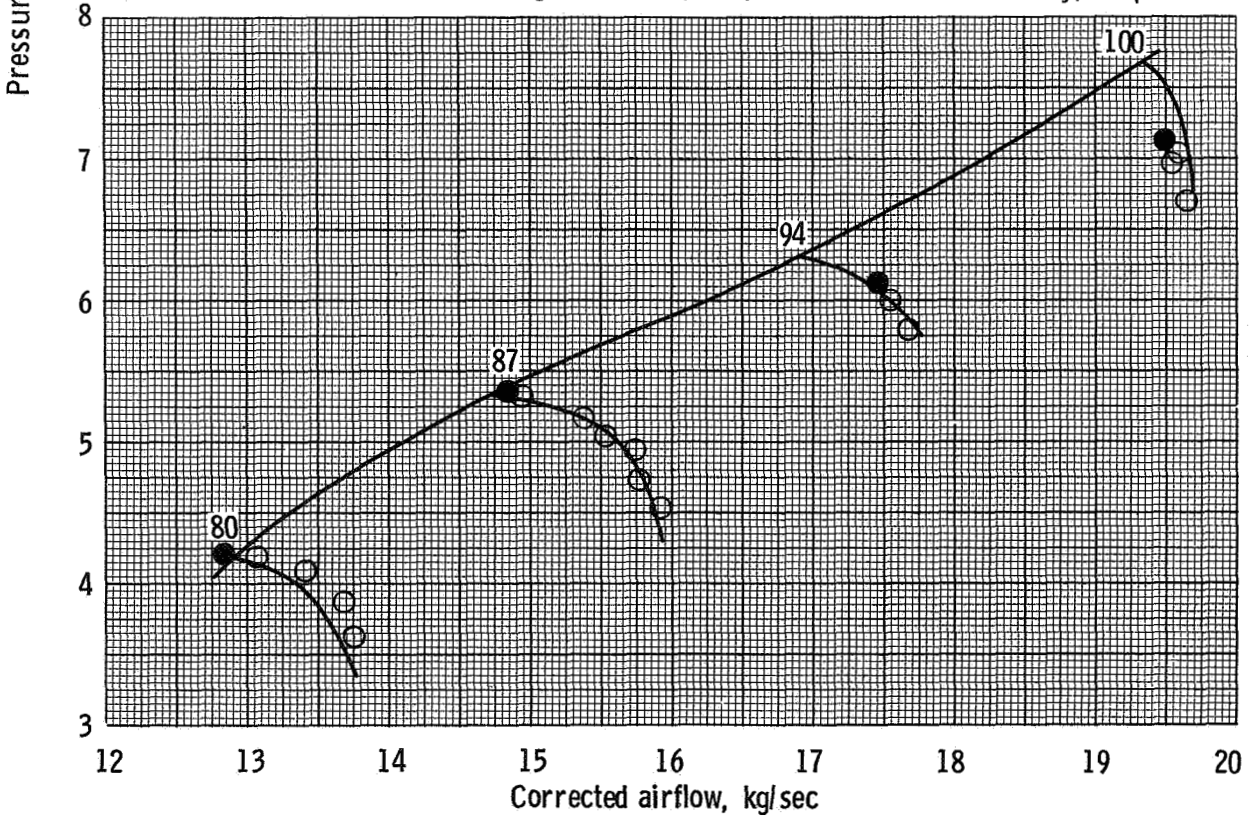

(h) Circumferential distortion; angle of extent, 30^0; distortion screen density, 42 percent.

Figure 7. - Continued.

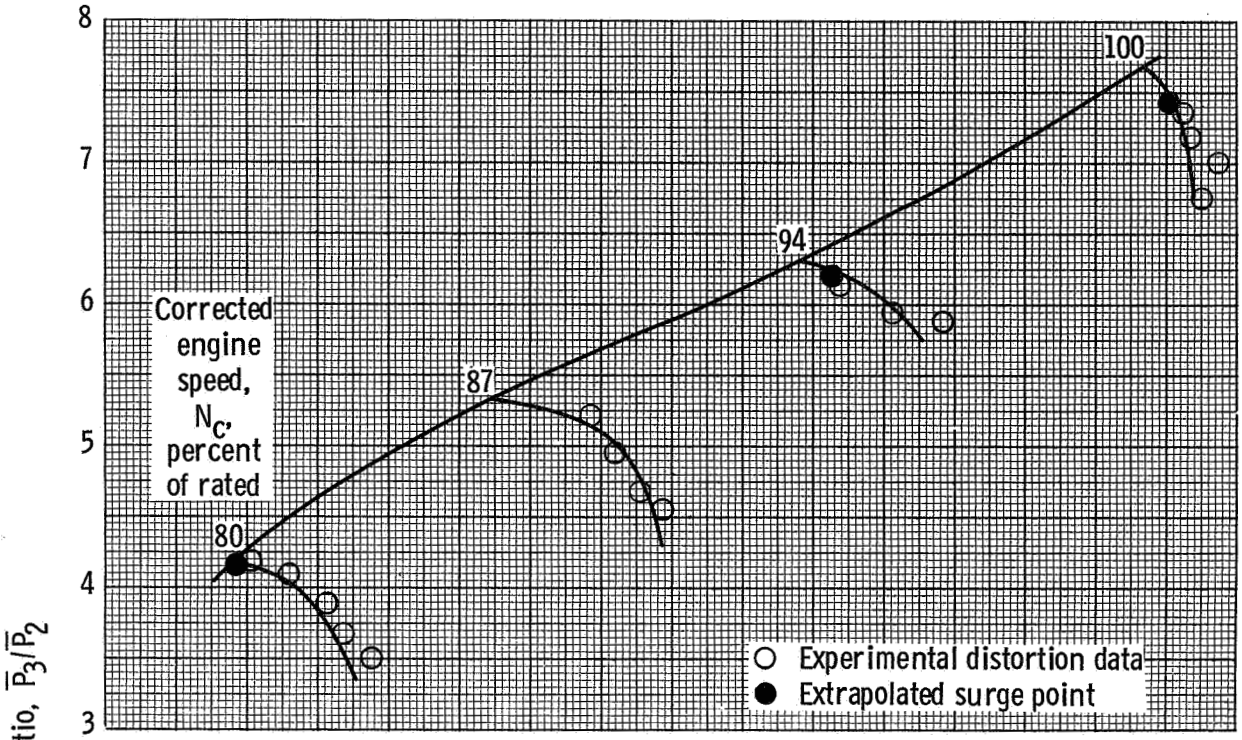

(i) Circumferential distortion; angle of extent, 180^0; distortion screen density, 26 percent.

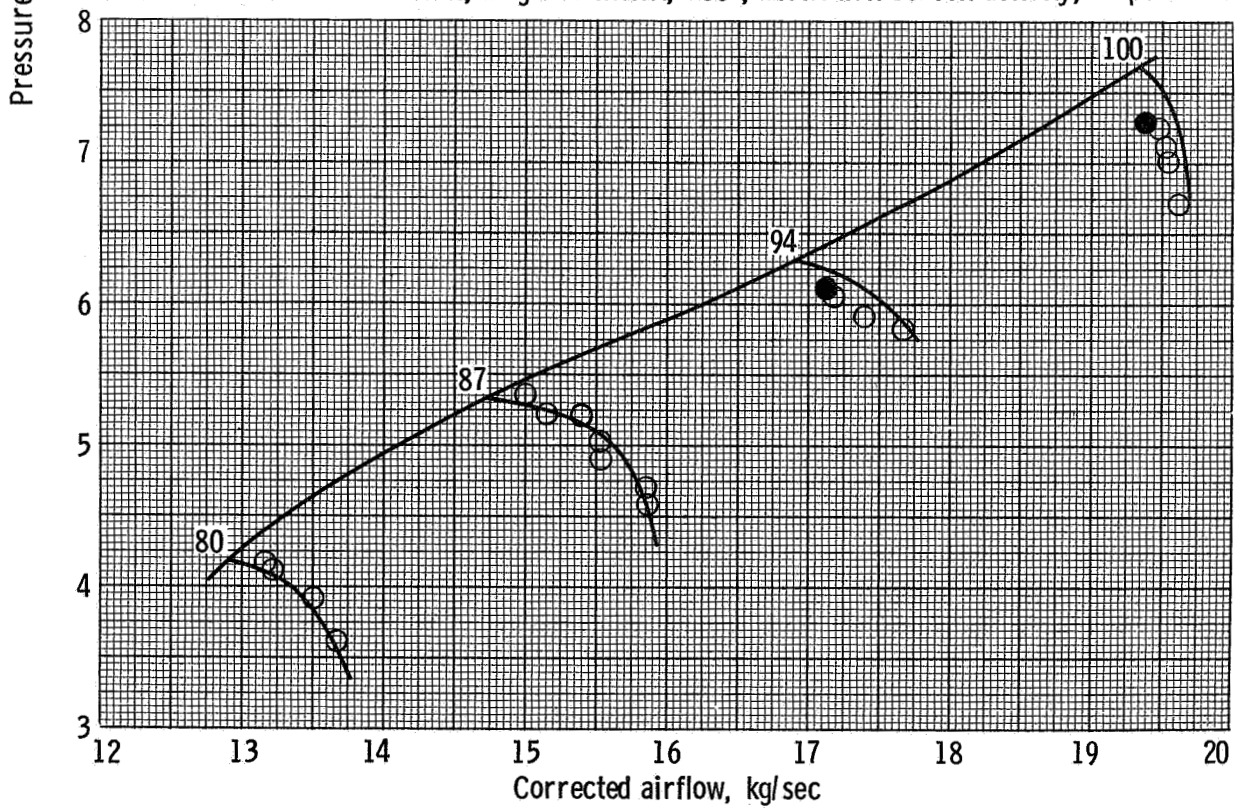

(j) Circumferential distortion; angle of extent, 90^0; distortion screen density, 26 percent.

Figure 7. - Continued.

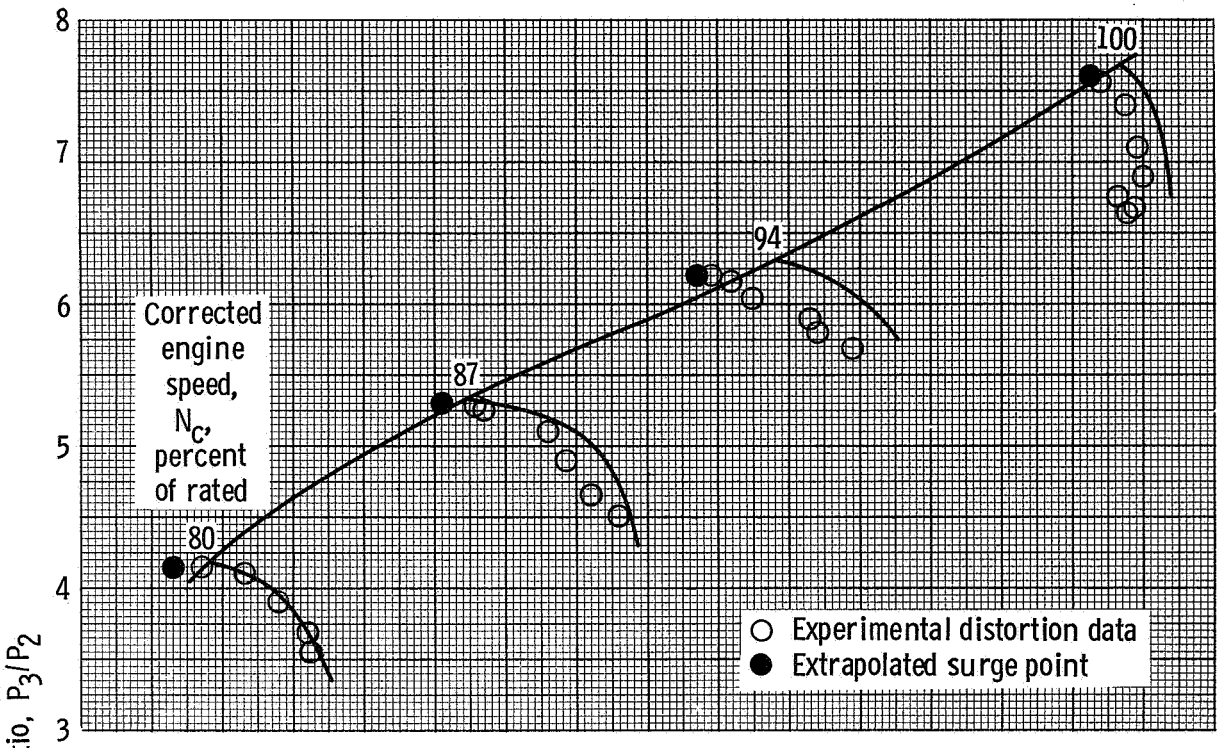

(k) Hub-radial distortion; 40 percent spoiled area; distortion screen density, 49 percent.

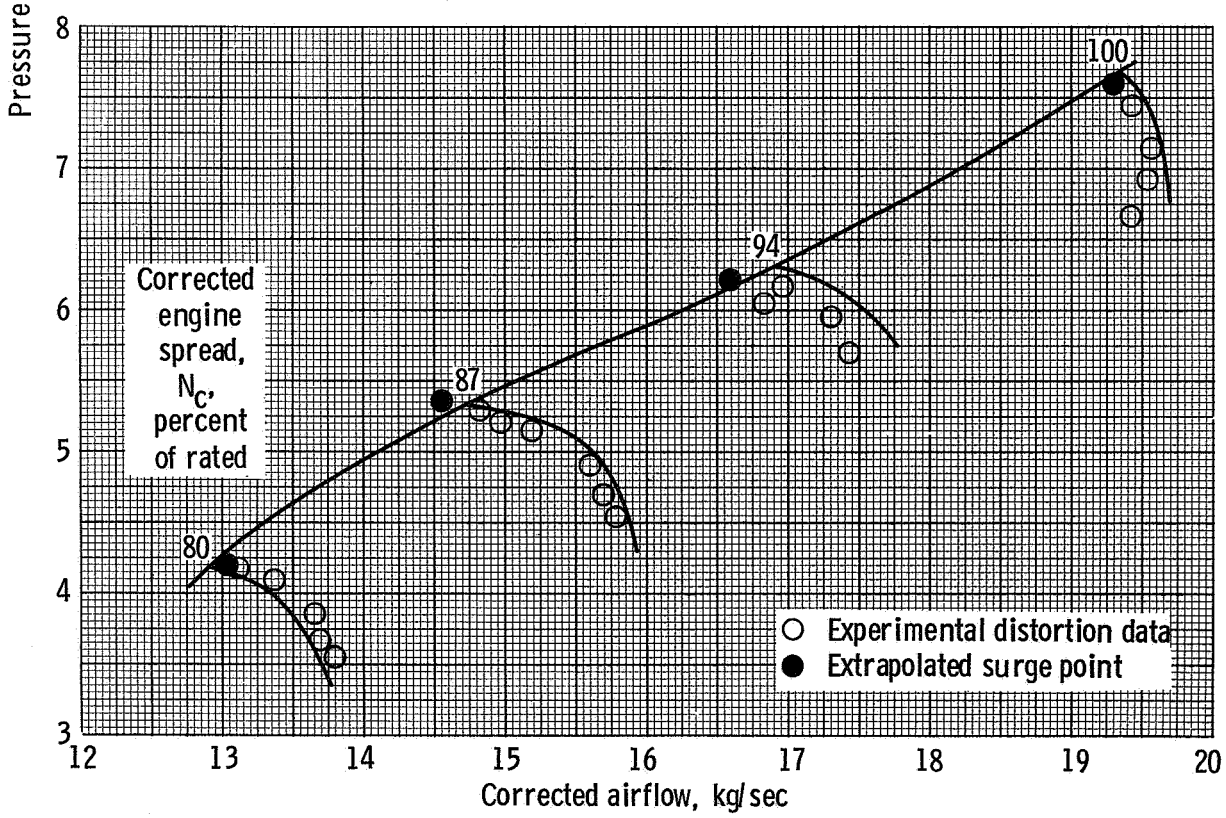

(l) Hub-radial distortion; 40 percent spoiled area; distortion screen density, 42 percent.

Figure 7. - Continued.

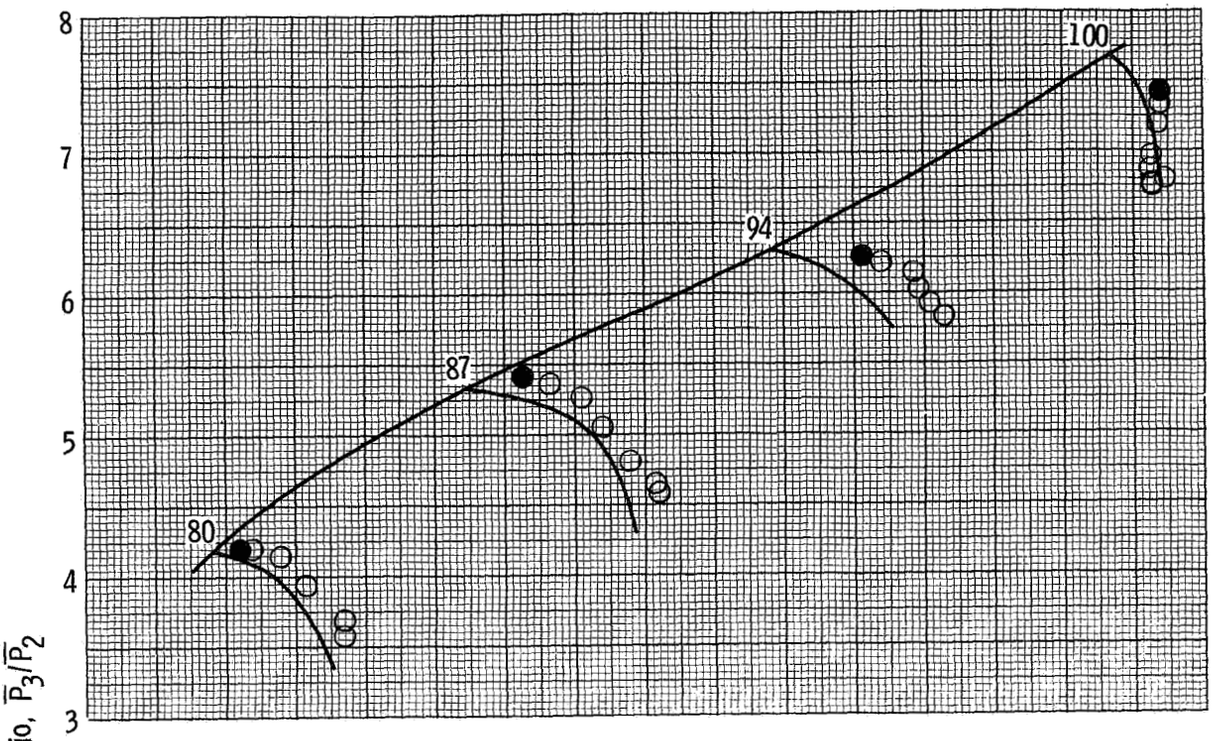

(m) Tip-radial distortion; 40 percent spoiled area; distortion screen density, 49 percent.

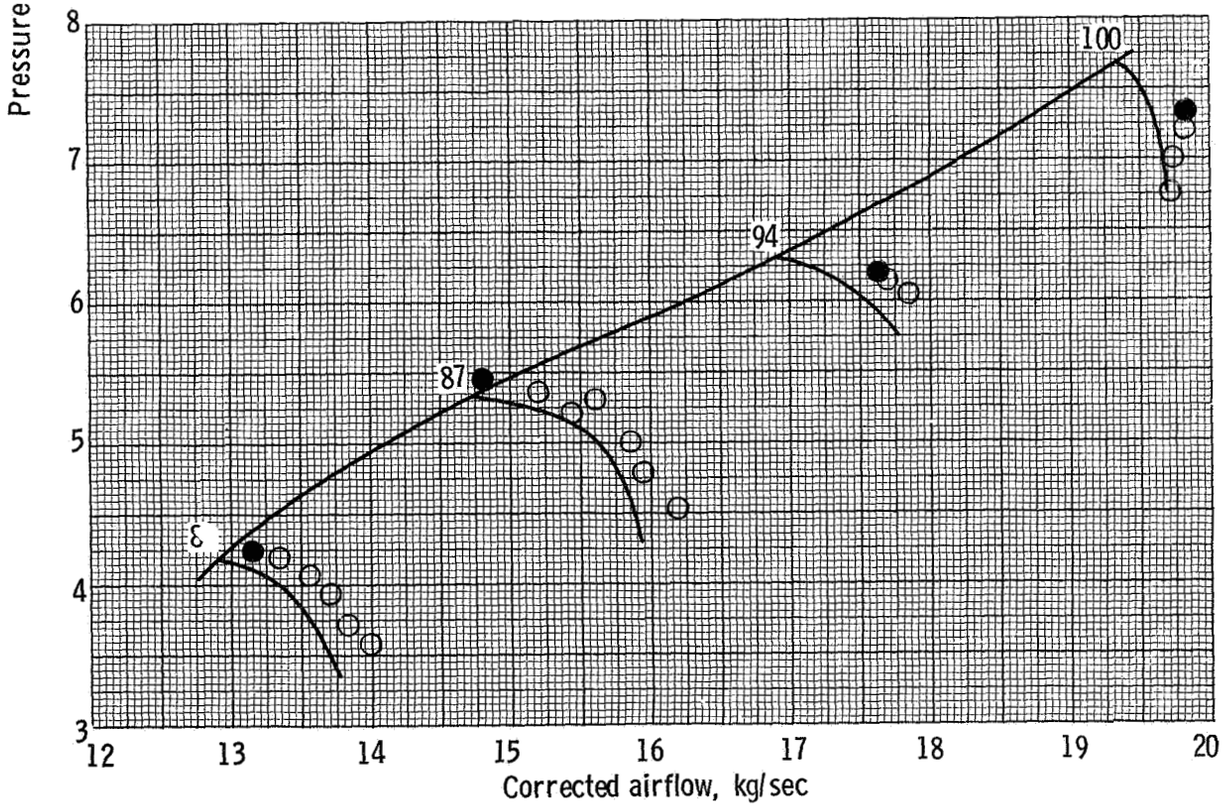

(n) Tip-radial distortion; 40 percent spoiled area; distortion screen density, 42 percent.

Figure 7. - Concluded.